

M. Ediger,¹ G. Bester,² B. D. Gerardot,¹ A. Badolato,³ P. M. Petroff,³ K. Karrai,⁴ A. Zunger,² and R. J. Warburton¹

¹ School of Physics, University of Bristol, Bristol, UK
² Department of Physics, University of Colorado, Boulder, CO, USA
³ Department of Physics, University of Colorado, Boulder, CO, USA
⁴ Department of Physics, University of Colorado, Boulder, CO, USA

(Received 26 June 2006; published 19 January 2007)

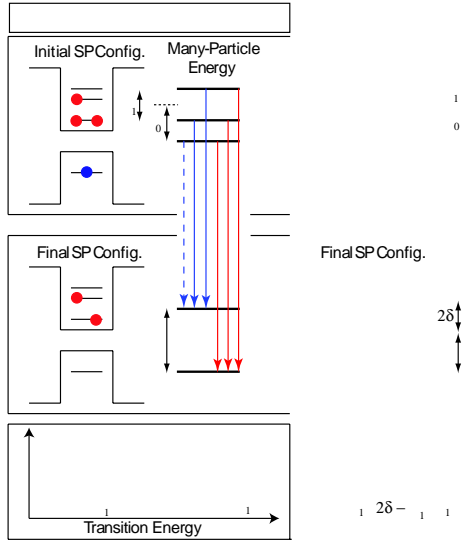
fluctuations were evaluated by measuring 10 dots from the InGaAs sample in the band 1.29–1.31 V and a few InAs dots in the band 1.04–1.06 V.

We have calculated the optical properties of both InAs and InGaAs quantum dots with the empirical pseudopotential method with a configuration interaction treatment of correlations [15]. The crystal potential is calculated as a superposition of atomic screened potentials v_α (of atom type α) at each relaxed atomic position \mathbf{R}_{an} (where n is the lattice site index): $V(\mathbf{r}) = \sum_{an} v_\alpha(\mathbf{r} - \mathbf{R}_{an})$. The description of the dots and its wetting layer in terms of the set $\{\mathbf{R}_{an}\}$ guarantees that the symmetries are resolved even at the atomistic level. The Hamiltonian is solved in a single-particle basis consisting of multiple Bloch states spread throughout the Brillouin zone. We include piezoelectricity in our calculations using first and second order effects [16]. The few-particle states, excitons and charged excitons, are calculated using a configuration interaction approach, where the Coulomb and exchange integrals are calculated explicitly from the single-particle wave functions. The distinction between short-range and long-range, or between isotropic and anisotropic electron-hole exchange does not arise. We use the available geometrical and structural data on the real dots as input to the theory: we model lens-shaped 25 nm diameter $\text{In}_{0.6}\text{Ga}_{0.4}\text{As}$ and InAs dots sitting on 2 monolayers of wetting layer with heights 3.5 and 2 nm, respectively. The calculated X^0 emission energies are 1.25 and 1.07 eV, matching the experimental X^0 PL energies, suggesting that these structures are good representations of the real ones. While the macroscopic symmetry is $D_{\infty v}$, the real symmetry is reduced to C_{2v} by

the atomistic symmetry of the zinc blende lattice, leading to the inequivalence of the $[110]$ and $[\bar{1}\bar{1}0]$ directions. The neutral exciton X^0 made of the fundamental electron (e_0) and hole (h_0) levels has four states: a lower dark doublet split slightly by band-mixing effects, and at energy Δ_0 above, a bright doublet split by Δ_1 .

Figure 1(a) shows a schematic of the calculated initial and final states of the X^{2-} transitions. On the left, we depict the dominant single-particle configurations, $h_0^1 e_0^2 e_1^1$ for the initial state and $e_0^1 e_1^1$ for the final state. Many such states interact, producing the many particle energy ladder shown on the right. The initial many-body states are split by electron-hole exchange. The splitting between the uppermost initial states, E_b and E_c , is labeled Δ_1 , and the splitting between the average of E_b and E_c and the doubly degenerate E_a is labeled Δ_0 . The final many-body states are split by electron-electron exchange $2X$ into a singlet state E_S and nearly degenerate triplet states E_T . For X^{2-} , the calculated Δ_1 and Δ_0 are comparable in magnitude (see Table I). For equal electron and hole orbitals, one would expect equal many-body spectra of X^{2-} and X^{2+} . This is not what the calculation reveals. Figure 1(b) shows the corresponding calculation for X^{2+} . The initial configuration, $h_0^2 h_1^1 e_0^1$, and the final configuration, $h_0^1 h_1^1$, are analogous to those for X^{2-} . Despite this, the X^{2+} initial states are more similar to those of X^0 than X^{2-} as states E_b and E_c are only slightly split. Furthermore, the X^{2+} final states are not the same as those of X^{2-} : the degeneracy of the triplet is lifted, resulting in two singlets split by 2δ and a low energy doublet. The dramatic difference between X^{2-} and X^{2+} is highlighted (Table I) by the fact that the calculated $\Delta_1(X^{2-}) \approx \Delta_0(X^{2-})$, yet $\Delta_1(X^{2+}) \ll \Delta_0(X^{2+})$.

Figure 1 allows an interpretation of the experimental results within the theoretical framework. All dots show the same fine-structure features. Figures 2(a) and 2(b) show measured X^{2-} PL spectra for two particular dots with close-to-average fine-structure splittings. For both InGaAs and InAs dots there are two groups of lines in the experiment, corresponding to transitions to the E_S and



E_T final states. In the higher energy group, there are three PL lines, reflecting the presence of the three initial states. The uppermost PL line is [110] polarized and at lower energy there is a $[1\bar{1}0]$ -polarized line. For each dot, these transitions are 100% polarized to within our experimental resolution of 5%, and the lowest energy line in the upper group is at most 20% polarized, lying almost at the same energy as the $[1\bar{1}0]$ -polarized transition. We prove that these large fine-structure splittings arise in the initial and not in the final states by verifying the theoretical expectation that the E_T state is triply degenerate. We do this by observing weak recombination between the $h_0^1 e_0^2 e_1^1$ and e_0^2 (not $e_0^1 e_1^1$) configurations where the final state has a closed S shell and is therefore a singlet. The PL however, Fig. 3, exhibits a large fine-structure splitting, with the same Δ_1 as for the open shell X^{2-} emissions in Fig. 2(a), proving that the triplet states are degenerate to within $10 \mu\text{V}$.

Several significant and surprising results emerge from the spectroscopy. First, Δ_1 for X^{2-} is considerably enhanced over that for the neutral exciton, X^0 . This is the case for every dot we have looked at. For the InGaAs dots, the average (standard deviation) is $\Delta_1(X^0) = 26(12) \mu\text{V}$; $\Delta_1(X^{2-}) = 73(10)$. For the particular dots in Fig. 2, $\Delta_1(X^0)$ is experimentally $26(<20) \mu\text{V}$, yet $\Delta_1(X^{2-})$ is $70(160) \mu\text{V}$ for the InGaAs (InAs) quantum dot. Second, for X^{2-} , the usual relationship $\Delta_1 \ll \Delta_0$ is broken. In Fig. 2, we measure $\Delta_1/\Delta_0 = 1.6(1.7)$ for InAs (InGaAs) dots [17] leading to the unusual situation that states E_b and

E_a are almost degenerate. Again, this is the case for all the dots we have measured.

In the lower energy group of X^{2-} PL lines, there is always another polarized doublet; example data in Figs. 2(a) and 2(b) [18]. These lines arise from the transition from E_b and E_c to E_S and are split by $\Delta_1(X^{2-})$. However, the polarizations of the lower group are now reversed, with the $[1\bar{1}0]$ - and the $[110]$ -polarized line at higher energy, as also observed for the transition to the closed shell in Fig. 3. This represents our third important experimental result.

We turn now to the X^{2+} PL which we have measured for the first time on an InAs dot; example data in Fig. 2(c). There is an unpolarized line with two fine-structure split doublets, each composed of two fully polarized lines, lying at lower energy. This is radically different to the X^{2-} PL, our fourth significant result. We point out several remarkable features of the X^{2+} spectrum. The most obvious is that the unpolarized emission line lies above the polarized emission lines. This is opposite to X^{2-} and also opposite to X^0 , where the so-called dark states (unpolarized in the limit of zero magnetic field [1]) lie beneath the so-called bright states (linearly polarized emission). Second, the X^{2+} spectral features are located in an energy band of just 3.5 meV compared to 10.1 meV for X^{2-} . This is a surprise as hole-hole Coulomb energies are larger than electron-electron Coulomb energies. Finally, the doublets are separated by just $\Delta_1(X^{2+}) = 20 \mu\text{V}$, which is small and only marginally enhanced over $\Delta_1(X^0) (<20 \mu\text{V})$, in complete contrast to $\Delta_1(X^{2-})$.

The theory (Fig. 4 and Table I

the exchange that can be seen as a dipole-dipole interaction, fundamentally different for an S - P exciton than for an S - S exciton. In the X^{2+} case, the initial state is similar to X^0 with a small value of Δ_1 . This can be understood by the isotropic character of the envelope of the hole P orbital (Fig. 1 of Ref. [3]). X^{2+} is therefore closer to X^0 , where both electron and hole envelopes are nearly isotropic, than to X^{2-} where the electron P wave function is highly anisotropic (Fig. 1 of Ref. [3]). The final state of the X^{2+} is drastically different to the final state of the X^{2-} . The two electrons in the X^{2-} final state follow the rules for spin- $\frac{1}{2}$ particles (triplet and singlet states) while the holes follow the addition of spin- $\frac{3}{2}$ particles. For dominantly heavy hole states, this leads to a twofold degenerate state with $J = 3$ and two singlets with $J = 0$ and $J = 2$.

To sum up, we have discovered new features in the fine structure (fine structure) of the X^{2-} exciton.

significant experimental results are paralleled by our theory. First, $\Delta_1(X^{2-})$ (91 μ V for the InGaAs dot and 158 μ V for the InAs dot) is significantly larger than $\Delta_1(X^0)$ (typically 10–50 μ V [3]). Second, $\Delta_1(X^{2-})$ is not significantly smaller than $\Delta_0(X^{2-})$ (as is typical for X^0) but similar (158 vs 132 μ V in InAs). We find that the near equivalence of $\Delta_0(X^{2-})$ and $\Delta_1(X^{2-})$ is a general feature in our calculations over a range of InGaAs and InAs dots. Third, the model also reproduces the polarizations of the X^{2-} PL: the calculated transitions are highly polarized but with reversed polarizations to E_S relative to E_T . Fourthly, the calculated X^{2+} spectrum also reproduces the most surprising experimental result, an unpolarized line at high energy with two lower-lying polarized doublets. The quantitative agreement between the energies defined and calculated theoretically and measured experimentally is very good with agreement to about $\sim 30\%$ (Table I). For the InAs dots, inclusion of the piezoelectricity improves somewhat the agreement with experiment, particularly for $\Delta_1(X^{2-})$ and δ for X^{2+} . Further theoretical investigations would benefit from a full morphological characterization of the InAs dots.

Our theory, unlike the effective Hamiltonian approach, allows us to offer, in addition to the full calculation, some simple explanations. For X^{2-} , the fine structure mainly originates from the spin interaction between a hole in an S orbital and an electron in a P orbital (the two additional electrons form a closed shell in the S orbital). This interaction has a different symmetry than the one in the X^0 exciton where both carriers have an S -like envelope function character, resulting in a substantially different Δ_1 . In the language of long- and short-range exchange, the large difference originates mainly from the long-range part of